Inorganic Chemistry

Forum Article

pubs.acs.org/IC

Reactivity of CO_2 Activated on Transition Metals and Sulfur Ligands

Katsuaki Kobayashi and Koji Tanaka*

Advanced Chemical Technology Center in Kyoto, Institute for Integrated Cell-Material Sciences, Kyoto University, Jibucho 105, Fushimi-ku, Kyoto 612-8374, Japan

ABSTRACT: Dicationic dicarbonyl $[Ru(bpy)_2(CO)_2]^{2+}$ (bpy = 2,2′-bipyridyl) exists as equilibrium mixtures with $[Ru(bpy)_2(CO)(COOH)]^+$ and $[Ru(bpy)_2(CO)(CO_2)]^0$ depending on the pH in H_2O. Those three complexes work as the precursors to CO, HCOOH production, and CO_2 carrier, respectively, in electro- and photochemical CO_2 reduction in aqueous solutions. However, $[Ru(bpy)_2(CO)_2]^{2+}$ loses the catalytic activity toward CO_2 reduction under aprotic conditions because $[Ru(bpy)_2(CO)_2]^{2+}$ is not regenerated from $[Ru(bpy)_2(CO)(CO_2)]^0$ in the absence of proton sources. Analogous monocarbonylruthenium complexes such as $[Ru(tpy)(bpy)(CO)]^{2+}$ and $[Ru(bpy)_2(qu)(CO)]^{2+}$ catalyze CO_2 reduction in the absence and presence of proton sources. Both complexes are reproduced through oxide transfer from the corresponding Ru−CO_2 to CO_2 in CO_2 reduction and produce the same amount of CO and CO_3^{2-} in the absence of proton donors. The reduction of CO_2 catalyzed by polypyridylrhenium complexes in the presence of proton sources takes place via essentially the similar mechanism as that in the case of ruthenium complexes. On the other hand, CO evolution in CO_2 reduction under aprotic conditions is ascribed to the dissociation of CO from a dimeric Re−C(O)OC(O)O−Re scaffold. Visible-light irradiation to a catalytic system composed of $[Ru(bpy)_2(CO)_2]^{2+}$/$[Ru(bpy)_3]^{2+}$/$Me_2NH_2^+$/Me_2NH as the catalyst, photosensitizer, proton donor, and nucleophile in addition to the electron donor, respectively, in CO_2-saturated CH_3CN selectively produces *N*,*N*-dimethylformamide without concomitant CO and HCOOH formation. Structurally robust μ_3-S of reduced metal−sulfur clusters provides a suitable site for reductive activation of CO_2 with retention of the framework. Indeed, CO_2 activated on μ_3-S of $[Fe_6Mo_2S_8(SEt)_3]^{5-}$ is fixed at the carbonyl carbon of thioesters trapped on a neighboring iron of the cluster, and α-keto acids are produced catalytically. Furthermore, two-electron reduction of $[(CpMe_n)_3M_3S_3]^{2+}$ (n = 1, M = Co; n = 5, M = Rh, Ir) creates the catalytic ability to produce oxalate through the coupling of two CO_2 molecules possibly activated on μ_3-S and a metal ion.

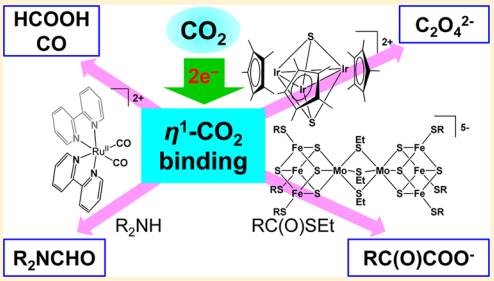

INTRODUCTION

Utilization of CO_2 as a C1 source would help mitigate global problems such as environmental degradation, energy shortage, and resource depletion caused by steady increases in fossil fuel and other natural resource consumption. Electrophilic attack of CO_2 toward amines and epoxy groups produces urea and carbonate derivatives.[1−4] Alkynes, alkenes, dienes, and benzene derivatives activated on transition metals react with CO_2 to produce a variety of pyrones, lactones, esters, and carboxylic acids.[5] Electrocarboxylation is a practicable methodology for CO_2 fixation.[6,7] Direct electrochemical reduction of CO_2 generates a $CO_2^{\bullet-}$ radical, which reacts with olefins and dienes, yielding carboxylate compounds. However, quite negative electrode potentials (<−2.10 V vs SCE) are required to reduce CO_2, so that reactive substrates such as organic halides and aryl compounds preferentially are reduced under CO_2. The resulting carbanions undergo an electrophilic attack of CO_2 to produce carboxylate compounds.[6−9] Alternatively, the reduction of nickel(II) and palladium(II) complexes proceeds at more positive potentials compared with the direct reduction of CO_2 and organic substrates. Electrophilic attack of CO_2 to organometallic complexes that are produced by the oxidative addition of organic halides to electrochemically generated nickel(0) and palladium(0) complexes also affords corresponding carboxylates.[10−14] Thus, electrocarboxylation through the reaction of reductively activated organic molecules with CO_2 has been well studied. On the other hand, useful organic compounds have hardly been obtained by the reaction of nonactivated organic molecules with CO_2 activated on metal complexes except for $CO_2^{\bullet-}$. Elucidation of the reactivity of CO_2 reductively activated on metal complexes would greatly serve for the utilization of CO_2 as a C1 building block under low energy consumption processes.

Most of the reduction products from photo- and electrochemical CO_2 reduction catalyzed by metal complexes have been limited to HCOOH and/or CO. Reaction mechanisms can be explained by the participation of two types of reaction intermediates in the catalytic cycle. The first is a metal−η^1-CO_2 complex formed by electrophilic attack of CO_2 on low oxidation states of metal centers (eq 1). The second is a

$$M^{n+} \underset{-CO_2}{\overset{+CO_2}{\rightleftharpoons}} M^{n+}\!-\!C(=O)O \underset{-H^+}{\overset{+H^+}{\rightleftharpoons}} M^{(n+2)+}\!-\!C(OH)=O \underset{+OH^-}{\overset{-OH^-}{\rightleftharpoons}} M^{(n+2)+}\!-\!CO \quad (1)$$

Special Issue: Small Molecule Activation: From Biological Principles to Energy Applications

Received: November 14, 2014
Published: May 15, 2015

DOI: 10.1021/ic502745u
Inorg. Chem. 2015, 54, 5085−5095

metal−H species formed by proton attack on reduced metal complexes or by hydrogen attack on metal centers (eq 2).Stepwise protonation of an oxygen of metal−η^1-CO_2

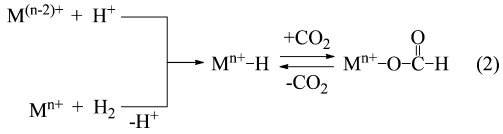

resulted in M−COOH and M−CO formation as precursors to HCOOH and CO. In the absence of a proton source, oxide transfer from metal−η^1-CO_2 to CO_2 also affords M−CO with generation of CO_3^{2-}. Insertion of CO_2 in M−H produces M−OC(O)H, which serves as a precursor to $HCOO^-$. It is worth noting that the reaction of nucleophiles with M−CO has significant importance in the incorporation of CO to organic substrates. However, M−CO bonds derived from reductive activation of CO_2 on metal complexes exclusively are cleaved without undergoing attack of nucleophiles on the bonds. In biological reactions, CO_2 is fixed to stable organic molecules with C−C bond formation. It still remains unclear whether CO_2 fixation in biological reactions proceeds via activation of either CO_2 or substrates or both. In contrast to reductive activation of CO_2 on transition-metal centers, structurally robust basic sites linked to redox centers of metal complexes may provide reasonable sites for not only condensation but also reductive activation of CO_2 with retention of the framework.

This review focuses on the reactivity of CO_2 activated on ruthenium and rhenium complexes and μ_3-S of metal−sulfur clusters with the goal of CO_2 reduction accompanied by C−C and C−N bond formation without the use of reactive substrates.

REDUCTIVE CONVERSION OF CO_2 ON RUTHENIUM COMPLEXES

The mechanism for conversion of CO_2 to CO using ruthenium carbonyl complexes bearing polypyridyl ligands as ancillary ligands has been well studied (Scheme 2).[15−18] Dicationic dicarbonyl $[Ru(bpy)_2(CO)_2]^{2+}$ (bpy = 2,2′- bipyridyl) has a unique function in the reversible conversion among CO_2, COOH, and CO via acid−base equilibrium.[15,19−22] Protonation of the low-valent Ru^0−η^1-CO_2 complex formed a Ru^{II}−COOH complex, which generated Ru^{II}−CO through protonation of the OH group (eq 3). The structures of $[Ru(bpy)_2(CO)X]^{n+}$ (X =

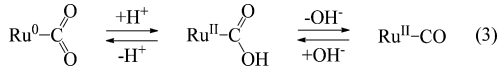

CO_2, COOH, CO; n = 0, 1, 2) were determined by X-ray crystal structural analysis.[23−25] The pK_a value of Ru−COOH was 9.6. Distributions of the three species in aqueous solutions were calculated based on the equilibrium constants[15] because the population of the three complexes was regulated by the pH (Figure 1).

Cyclic voltammetry (CV) of $[Ru(bpy)_2(CO)_2]^{2+}$ in 1:9 (v/v) *N*,*N*-dimethylformamide (DMF)/H_2O showed one irreversible broad cathodic wave at −0.95 V vs SCE under N_2, resulting from a two-electron redox reaction.[15] Bubbling CO_2 into the solution caused strong catalytic currents at potentials more negative than −1.4 V. Controlled potential electrolysis of $[Ru(bpy)_2(CO)_2]^{2+}$ in CO_2-saturated 9:1 (v/v) H_2O/DMF produced CO or HCOOH as CO_2 reduction products. The product selectivity depended on the pH; CO was produced

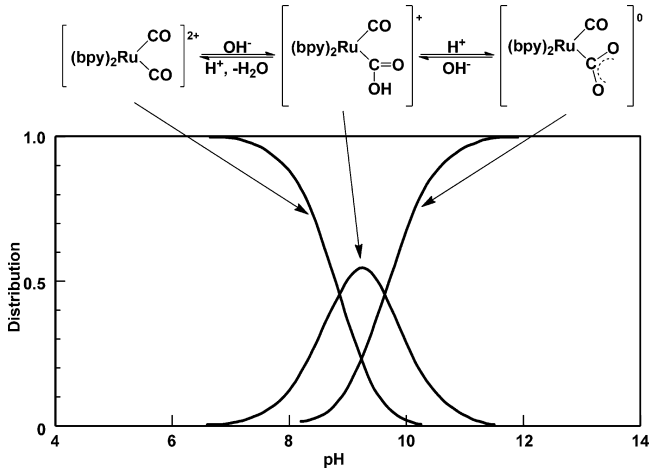

Figure 1. Distribution of the ruthenium species in H_2O at various pH values at 25 °C.

with 32% current efficiency, along with H_2 evolution, without HCOOH formation in 9:1 (v/v) H_2O/DMF (pH 6; Figure 2a). In contrast, nearly the same amounts of HCOOH and CO were produced together with H_2 (Figure 2b) at pH 9.5. Variation in the reduction products dependent on the pH (Figure 1) was attributed to the participation of Ru−CO and Ru−COOH species as precursors to CO and HCOOH in the catalytic cycle. The catalytic ability of $[Ru(bpy)_2(CO)_2]^{2+}$ toward CO_2 reduction decreased upon increasing alkalinity in 1:9 (v/v) DMF/H_2O solutions due to complete conversion of CO_2 to CO_3^{2-}. Electrochemical reduction of $[Ru(bpy)_2(CO)_2]^{2+}$ in the presence of Me_2NH_2Cl in CO_2-saturated CH_3CN selectively produced HCOOH (Figure 2c).[26] Differences in the reduction products (shown in Figure 2a−c) were associated with the distribution of the three ruthenium complexes, depending on the proton concentration (Scheme 1). Two-electron reduction of $[Ru(bpy)_2(CO)_2]^{2+}$ resulted in CO dissociation, and subsequent electrophilic attack of CO_2 on $[Ru(bpy)_2(CO)]^0$ produced $[Ru(bpy)_2(CO)(CO_2)]^0$, which existed as an equilibrium mixture with $[Ru(bpy)_2(CO)(COOH)]^+$ and $[Ru(bpy)_2(CO)_2]^{2+}$, depending on the proton concentration. The latter two acted as precursors to HCOOH and CO.

Ziessel et al. reported that electrodeposition of *trans*(Cl)-$[Ru(bpy)(CO)_2(Cl)_2]$ in a CH_3CN solution formed a polymeric $[Ru(bpy)(CO)_2]_n^0$ film on the electrode, which also catalyzed electrochemical CO_2 reduction.[27,28] A polymeric $[Ru(bpy)(CO)_2]_n^0$ film was also formed in electrolysis of $[Ru(bpy)_2(CO)_2]^{2+}$ in CH_3CN.[29] The most remarkable difference between discrete $[Ru(bpy)_2(CO)_2]^{2+}$ and the $[Ru(bpy)(CO)_2]_n^0$ film was the pH dependence in electrochemical CO_2 reduction.[30] As described above, electrolysis of $[Ru(bpy)_2(CO)_2]^{2+}$ under CO_2 afforded CO and HCOOH depending on the pH. On the contrary, the $[Ru(bpy)(CO)_2]_n^0$ film produced almost a single product in both acidic and basic conditions; the selectivity for the products between CO and HCOOH depended on the substituents of the bpy ligand involved in the polymeric ruthenium film.[30] Fabrication of the $[Ru(bpy)(CO)_2]_n^0$ film in the supramolecular complex composed of $[Ru(bpy)_2(CO)_2]_n$ and $[Ru(bpy)_3]_m$ scaffolds as the catalyst and photosensitizer, respectively, resulted in a substantial decrease in the catalytic activity toward photochemical CO_2 reduction.[31] Photochemical CO_2 reduction

DOI: 10.1021/ic502745u
Inorg. Chem. 2015, 54, 5085−5095

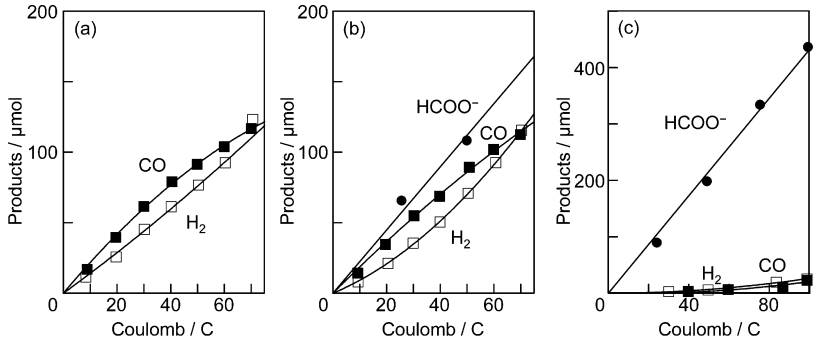

Figure 2. Plots of the amounts of products versus coulombs consumed in the electrolysis (−1.50 V vs SCE) of $[Ru(bpy)_2(CO)_2]^{2+}$ in CO_2-saturated (a) 9:1 (v/v) H_2O (pH 6.0)/DMF, (b) 9:1 (v/v) H_2O (pH 9.5)/DMF, and (c) dry CH_3CN containing 0.1 M Me_2NH_2Cl.

Scheme 1. CO_2 Reduction Catalyzed by $[Ru(bpy)_2(CO)_2]^{2+}$ in Aqueous Solutions

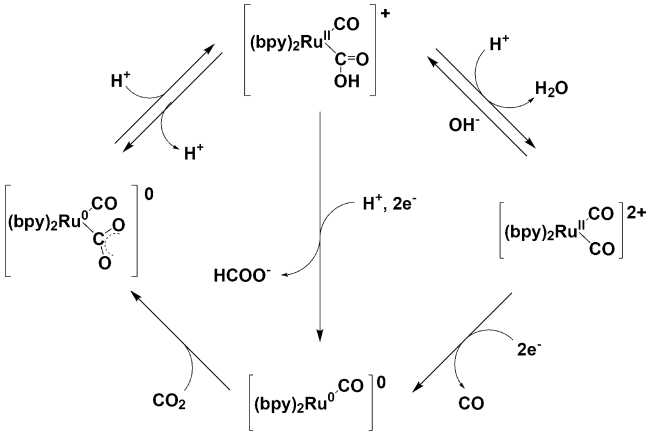

Scheme 2. Proposed Reaction Mechanism for CO_2 Reduction by a Ruthenium Carbonyl Polymer

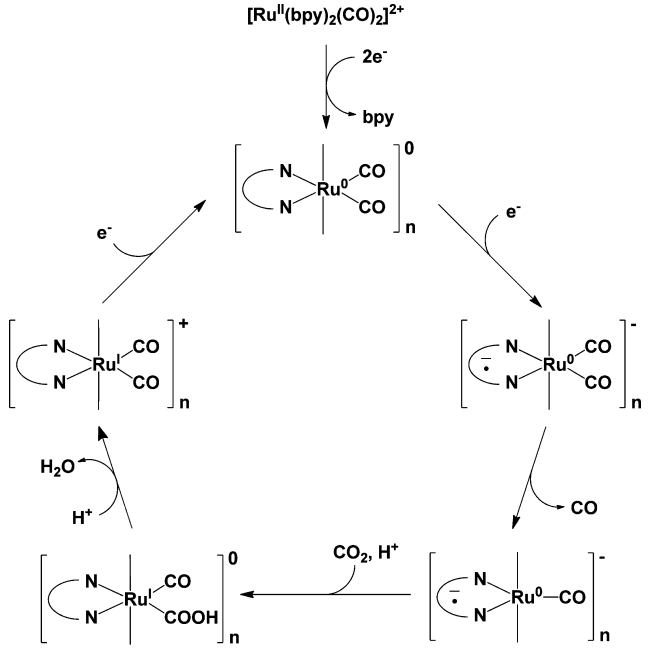

catalyzed by the supramolecular complexes showed the tendency for bpy dissociation from the catalyst framework with a decrease of the number of photosensitizers, indicating that the decrement of electron supply from the photosensitizer to the catalyst induces dissociation of bpy in CO_2 reduction. Release of bpy from the catalyst framework, forming polymeric $[Ru(bpy)(CO)_2]_n^0$ in the supramolecular complexes, resulted in a drastic decrease of the catalytic activity in photochemical CO_2 reduction.

Colorless $[Ru(bpy)_2(CO)_2]^{2+}$ cannot catalyze photochemical CO_2 reduction under visible-light irradiation. The catalytic system composed of $[Ru(bpy)_2(CO)_2]^{2+}/[Ru(bpy)_3]^{2+}$/triethanolamine (TEOA) as the catalyst, photosensitizer, and sacrificial electron donor, respectively, produced HCOOH in CO_2-saturated DMF under visible-light irradiation.[32] A similar photocatalytic system using 1-benzyl-1,4-dihydronicotinamide instead of TEOA under the same reaction conditions did not afford any reduction products, whereas the addition of H_2O to the reaction mixture caused photochemical CO_2 reduction to generate CO and $HCOO^-$.[32,33] In addition, the $CO/HCOO^-$ ratio increased with an increase of H_2O concentrations.[32] Thus, the proton source was the essential component in electro- and photochemical CO_2 reduction catalyzed by $[Ru(bpy)_2(CO)_2]^{2+}$ because the selectivity for CO and HCOOH formation was dependent on the acid−base equilibrium of $[Ru(bpy)_2(CO)(CO_2)]$, $[Ru(bpy)_2(CO)(COOH)]^+$, and $[Ru(bpy)_2(CO)_2]^{2+}$ in a solution (Scheme 1).

The IR spectra of $[Ru(bpy)_2(CO)(\eta^1\text{-}CO_2)]$ in CH_3CN and dimethyl sulfoxide (DMSO) under N_2 were not influenced by bubbling CO_2 into the solution.[34] In contrast, the addition of $(NMe_4)_2CO_3$ to a DMSO solution of $[Ru(bpy)_2(CO)_2]^{2+}$ resulted in the slow formation of $[Ru(bpy)_2(CO)(\eta^1\text{-}CO_2)]$, although the latter slowly decomposed because of the relative instability of the Ru−η^1-CO_2 scaffold without interaction with Lewis acids.[23,24,34,35] This result indicates the occurrence of oxide transfer from CO_3^{2-} to $[Ru(bpy)_2(CO)_2]^{2+}$ (eq 4). Such an unusual oxide transfer from CO_3^{2-} to a metal−CO complex also has been reported in the reaction of a dinuclear iridium complex with CO_3^{2-} via another mechanism.[36]

$$[Ru(bpy)_2(CO)_2]^{2+} + CO_3^{2-} \rightleftarrows [Ru(bpy)_2(CO)(\eta^1\text{-}CO_2)]^0 + CO_2 \quad (4)$$

The ^{13}C NMR spectra revealed 1:1 adduct formation between $[Ru(bpy)_2(^{12}CO)(^{13}CO)]^{2+}$ and $(NMe_4)_2CO_3$ in DMSO-d_6 (eq 5, center).[34] The structure of the adduct of CO_3^{2-} and $[Ru(bpy)_2(CO)_2]^{2+}$ was essentially the same as that of $[Ru(bpy)_2(CO)(\eta^1\text{-}CO_2)]$ stabilized with a Lewis acid because the chemical shift of the Ru−$^{13}COOCO_2$ signal was very close to that of $[Ru(bpy)_2(CO)(\eta^1\text{-}^{13}CO_2)]^0$. The direction of the oxide from Ru−CO_2 to CO and back, therefore, is regulated by cleavage of either the RuC(O)O−

DOI: 10.1021/ic502745u
Inorg. Chem. 2015, 54, 5085−5095

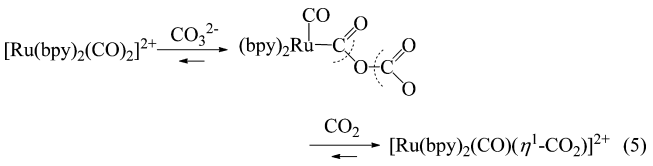

CO_2 or RuCO−CO_3 bond of the 1:1 adduct (eq 5). The pK_a values of the conjugated acid $[Ru(bpy)_2(CO)(C(O)OH)]^+$ (9.6)[15] and $HOCO_2$ (10.3) indicated that $[Ru(bpy)_2(CO)(\eta^1\text{-}CO_2)]$ was less basic than CO_3^{2-}. Therefore, when the 1:1 adduct formed between $[Ru(bpy)_2(CO)_2]$ and CO_3^{2-} and between $[Ru(bpy)_2(CO)(\eta^1\text{-}CO_2)]$ and CO_2, RuC(O)O−CO_2 bond cleavage was favored over RuC(O)−OCO_2 bond fission.

In contrast to $[Ru(bpy)_2(CO)_2]^{2+}$, monocarbonyl $[Ru(tpy)(bpy)(CO)]^{2+}$ (tpy = 2,2′:6′,2″-terpyridyl) and $[Ru(bpy)_2(qu)(CO)]^{2+}$ (qu = quinoline) have the ability to catalyze electrochemical CO_2 reduction in the presence and absence of a proton source.[37] The product of CO_2 reduction catalyzed by those complexes was CO due to oxide transfer from the electron-rich M−CO_2 scaffold to CO_2 (reductive disproportionation of CO_2) in the absence of a proton source.[36,38−41] Thus, the inability for oxide transfer from $[Ru(bpy)_2(CO)(CO_2)]^0$ to CO_2 eliminates the catalytic ability of $[Ru(bpy)_2(CO)_2]]^{2+}$ toward CO_2 reduction in the absence of a proton source.

■ ACTIVATION OF CO_2 ON RHENIUM COMPLEXES

Since the discovery that *fac*-Re(bpy)$(CO)_3$Cl functions as the catalyst and photosensitizer in photochemical CO_2 reduction,[42] a large number of CO_2 reductions using *fac*-Re(bpy-R)$(CO)_3$X (bpy-R, 4,4′-disubstituted-2,2′-bipyridyl; X = anionic ligand or solvent) have been reported.[42−46] For CO evolution, two types of reductive conversion of CO_2 to CO on rhenium have been proposed:[43] one is an acid−base equilibrium, and the other is disproportionation of Re−CO_2 under CO_2.[47,48] The two-electron-reduced form of $[Re(bpy\text{-}R)(CO)_3X]$ (X = anionic ligand or solvent) released a monodentate ligand X. Electrophilic attack of CO_2 on the resulting $[Re(bpy\text{-}R)(CO)_3]^-$ produced $[Re(bpy\text{-}R)(CO)_3(CO_2)]^-$. The acid−base equilibrium of the Re−CO_2 scaffold promoted conversion from CO_2 to CO similar to that of Ru−CO, as shown in Scheme 1.[48,49] The rate of CO_2 reduction followed second-order kinetics with regard to the H^+ concentration. On the basis of the H/D kinetic isotope effect in CO_2 reduction, protonation of Re−CO_2 and the subsequent dehydroxylation of Re−C(O)OH is involved in the rate-determining step.[49] Recently, the process for protonation of the Re−CO_2 group was detected by IR spectroelectrochemistry[50,51] and cold-spray ionization spectrometry.[52]

Direct oxide transfer from electron-rich Ru−CO_2 to CO_2 induced reductive conversion of CO_2 to CO in the absence of proton sources (reverse reaction of eq 4). In contrast, reductive disproportionation of CO_2 on rhenium complexes proceeded through the association of two rhenium complexes in the cycle (Scheme 3).[47,51,53] CO_2 reacted successively with two $[Re(bpy\text{-}R)(CO)_3]^0$ to form a CO_2-bridged rhenium dimer (Scheme 3C). Insertion of a second CO_2 molecule into the CO_2-bridged

Scheme 3. Proposed Mechanism for Reductive Disproportionation of CO_2 Catalyzed by a Rhenium Carbonyl Compound

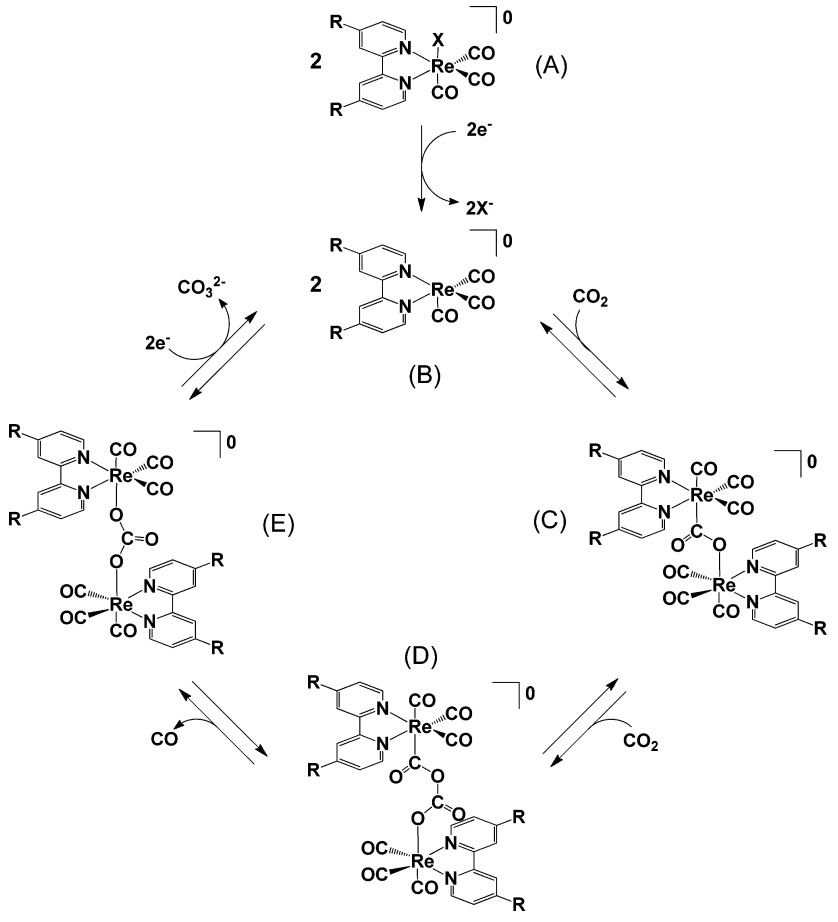

DOI: 10.1021/ic502745u
Inorg. Chem. 2015, 54, 5085−5095

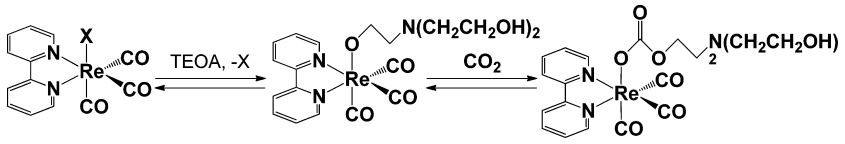

Figure 3. CO_2 capture on the rhenium complex assisted by TEOA.

dimer,[54] which resulted in CO emission with formation of a carbonate-bridged dimer (Scheme 3D). Subsequent reduction of the carbonate-bridged dimer regenerated the pentacoordinated rhenium complex and CO_3^{2-}. Recently, Kubiak et al. reported that a noncovalently associated rhenium dimer complex effectively enhanced CO_2 reduction through reductive disproportionation.[51] Also, the rate of CO_2 reduction was not significantly improved by the addition of a proton source.

The three components—catalyst, photosensitizer, and electron donor—greatly influence the efficiency of photochemical CO_2 reduction. Recent developments have enabled substantial improvements in photochemical CO_2 reduction.[55−60] A quantum yield of CO of up to 82% was achieved under visible-light irradiation,[61] using 1,3-dimethyl-2-phenyl-2,3-dihydro-1*H*-benzo[*d*]imidazole[62] and supramolecular catalysts linked with photosensitizers. In addition, a new role for TEOA in photochemical CO_2 reduction was elucidated. Substitution of a solvated molecule by TEOA with an oxygen atom on rhenium and subsequent CO_2 insertion into the Re−O bond afforded the Re−OCO_2 scaffold, which effectively acted as the CO_2 carrier in photochemical reduction (Figure 3).[63]

NUCLEOPHILIC REACTION TO M−CO COMPOUNDS

Reactions of nucleophiles with oxidatively activated M−CO are widely used to incorporate CO to organic substrates. For example, $[Ru(bpy)_2(CO)_2]^{2+}$ reacted with $NaBH_4$ to produce $[Ru(bpy)_2(CO)(CHO)]^+$ and $[Ru(bpy)_2(CO)(CH_2OH)]^+$.[64−68] Hydrolysis of the latter afforded MeOH. Therefore, reductive conversion of CO_2 to CO on metals, followed by attack of a nucleophile on the resultant M−CO scaffold prior to CO evolution, is a feasible pathway for preparing valuable molecules using CO_2 as a C1 building block. However, reduction of $[Ru(bpy)_2(CO)_2]^{2+}$ using strong hydride donors was problematic in the utilization of CO_2 because CO_2 was reduced to $HCOO^-$ by $NaBH_4$. Thus, strong nucleophiles are not useful substrates in the utilization of CO_2 as a C1 source by considering the Lewis acidity of CO_2.

Amines interacted weakly with CO_2 to form a 1:1 CO_2 adduct. Primary amine attacks on a carbonyl carbon of $[(C_5H_5)W(CO)_4]PF_6$ and $[(C_5H_5)Mo(CO)_4]PF_6$ afforded $[(C_5H_5)W(CO)_3(C(O)NHR)]$ and $[(C_5H_5)Mo(CO)_3(C(O)NHR)]$, respectively.[69] The second attack of a primary amine on the carbamoyl groups generated urea derivatives. A carbonyl carbon of $[Ru(bpy)_2(CO)_2]^{2+}$ also smoothly underwent an attack of Me_2NH to form $[Ru(bpy)_2(CO)(C(O)NMe_2)]^+$ (eq 6), which smoothly regenerated $[Ru(bpy)_2(CO)_2]^{2+}$ with dissociation of Me_2NH under reduced pressure.[70,71]

$$[Ru(bpy)_2(CO)_2]^{2+} + 2Me_2NH \rightleftarrows [Ru(bpy)_2(CO)(C(O)NMe_2)]^+ + Me_2NH_2^+ \quad (6)$$

The controlled potential electrolysis of $[Ru(bpy)_2(CO)_2]^{2+}$ in CO_2-saturated CH_3CN containing nBu_4NClO_4, Me_2NH, Me_2NH_2Cl, and Na_2SO_4 as a dehydration agent at −1.30 vs SCE produced DMF in addition to HCOOH, CO, and H_2, with current efficiencies of 21.4, 75.7, 1.0, and 0.7%, respectively (Figure 4).[70] Note that $Me_2NH_2^+$ acted as the proton source in the reduction of CO_2 and that $[Ru(bpy)_2(CO)(C(O)NMe_2)]^+$ (eq 6) acted as the precursor to DMF.

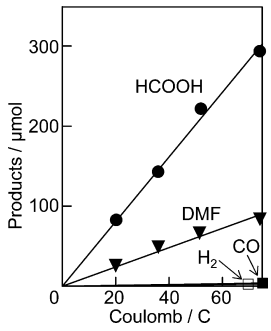

Figure 4. Plots of the amounts of products versus coulombs consumed in the electrolysis (−1.30 V vs SCE) of $[Ru(bpy)_2(CO)_2]^{2+}$ in CO_2-saturated dry CH_3CN containing Me_2NH_2Cl and Me_2NH.

DIALKYLFORMAMIDE PRODUCTION BY PHOTOCHEMICAL REDUCTION

Electrochemical reduction conducted at −1.30 vs SCE was easily applied to photochemical reduction using $[Ru(bpy)_3]^{2+}$ as a photosensitizer because $[Ru(bpy)_3]^+$ ($E_{1/2}$ = −1.37 V vs SCE) was generated through reductive quenching of $[Ru(bpy)_3]^{2+*}$ by reagents that provided electrons to the catalyst. Photochemical reduction in the presence of $[Ru(bpy)_3]^{2+}$, without the use of an electrolyte (nBu_4NClO_4) under the same conditions of electrochemical CO_2 reduction, produced 131 μmol of DMF and a trace amount of HCOOH upon 12 h irradiation of visible light (300 W xenon lamp; 385−750 nm).[71] The results of dialkylformamide formation by photochemical CO_2 reduction using various dialkylamines (R_2NH, where R = Et, *n*Pr, *i*Pr, and *n*Bu) and their ammonium salts are summarized in Table 1. Dialkylformamide derivatives from

Table 1. Products of Photochemical CO_2 Reduction Catalyzed by $[Ru(bpy)_2(CO)_2]^{2+}$ (0.5 mM) in the Presence of Dialkylamines and Their Ammonium Salts[a]

		products/μmol		
amine	ammonium	CO	HCOOH	R_2NCHO
Me_2NH	Me_2NH_2Cl	ND	trace	131
Et_2NH	$Et_2NH_2PF_6$	4.6	14	29
nPr_2NH	$nPr_2NH_2PF_6$	2.6	45	14
iPr_2NH	$iPr_2NH_2PF_6$	ND	21	ND
nBu_2NH	$nBu_2NH_2PF_6$	2.9	73	25

[a]The concentrations of dialkylamines and their ammonium salts were 0.5 and 0.2 M, respectively. 5 mM $[Ru(bpy)_3]^{2+}$.

DOI: 10.1021/ic502745u
Inorg. Chem. 2015, 54, 5085−5095

Et_2NH, nPr_2NH, and nBu_2NH were accompanied by HCOOH formation. The main products resulting from the transition of dialkylformamide to HCOOH depended on the steric hindrance of the dialkyl groups. When iPr_2NH was used, no iPr_2NCHO was produced possibly because of the steric hindrance of the two iPr groups on the nucleophilic attack at the carbonyl carbon of $[Ru(bpy)_2(CO)_2]^{2+}$. The product ratio of R_2NCHO to HCOOH depended on the dialkylamine; DMF was selectively produced upon the addition of Me_2NH. The rates of adduct formation between $[Ru(bpy)_2(CO)_2]^{2+}$ and R_2NH determined by spectral changes after mixing in CH_3CN followed first-order kinetics with respect to R_2NH concentrations (Table 2). The reaction rate between $[Ru(bpy)_2(CO)_2]^{2+}$ and Me_2NH was approximately 2 orders of magnitude compared with that obtained with Et_2NH, nPr_2NH, or nBu_2NH. On the basis of the results shown in Tables 1 and 2, the selectivity for dialkylformamide formation is regulated by the reaction rate of the nucleophilic attack of the dialkylamine on $[Ru(bpy)_2(CO)_2]^{2+}$.[71]

Table 2. Reaction Rate Constants between $[Ru(bpy)_2(CO)_2]^{2+}$ (0.5 mM) and Various Dialkylamines (0.5 M)

amine	Me_2NH	Et_2NH	nPr_2NH	nBu_2NH
k_{obs}/s^{-1}	165	4.4	2.7	4.2

Relative rate differences between the nucleophilic attack of Me_2NH and electron injection to $[Ru(bpy)_2(CO)_2]^{2+}$ in electro- and photochemical CO_2 reduction greatly influence DMF formation. In electrochemical reduction, electrodes rapidly and continuously provide electrons to the complex existing near the electrode, while most of the ruthenium complexes existing far from the electrode are inert to CO_2 reduction. In contrast, photochemically generated $[Ru(bpy)_3]^+$ provided electrons to all ruthenium complexes in homogeneous solutions, but the electron supply was a stepwise and slow process. When the rate of electron flow to the Ru−COOH complex is much faster than the rate of conversion to Ru−CO through acid−base equilibrium, HCOOH becomes the main product, as observed in electrochemical CO_2 reduction. However, a limited electron supply to ruthenium complexes in photochemical reduction gives rise to adequate time for conversion from Ru−COOH to Ru−CO. Selective Me_2NCHO generation in photochemical CO_2 reduction indicates that the rate of attack of Me_2NH to Ru−CO is much faster than that of reductive Ru−CO bond cleavage caused by electron injection to the complex.

The oxo affinity of Li^+ also influenced DMF generation. Photochemical CO_2 reduction in the presence of 0.1 M $LiBF_4$ along with Me_2NH and $Me_2NH_2^+$ resulted in a substantial decrease in DMF production (9.5 μmol) and the production of a small amount of HCOOH (15 μmol).[71] This result clearly indicates that conversion from Ru−CO_2 to Ru−CO (eq 3) was depressed significantly by stabilization of the Ru−η^1-CO_2 scaffold with Li^+. Thus, generation of Ru−$C(O)NMe_2$ as the precursor to DMF was blocked by Li^+. The proposed mechanism for catalytic dialkylformamide formation is shown in Scheme 4. The selectivity of HCOOH, CO, and R_2NCHO generation during CO_2 reduction correlated with the relative rates of the following three reactions: (1) CO_2, COOH, and CO conversion on ruthenium (eq 3), (2) reductive Ru−COOH and R−CO bond cleavage induced by electron injection to those frameworks, and (3) attack of R_2NH on the Ru−CO scaffold (eq 6). Li^+ apparently suppressed conversion from Ru−CO_2 to Ru−CO. Because conversion from Ru−CO_2 to Ru−$C(O)NR_2$ through Ru−CO is regulated by the concentrations of both the protons and alkyl group of R_2NH, rapid electron injection to Ru−COOH and Ru−CO was not necessary to improve the selectivity for $R_2NC(O)H$ generation. Thus, photochemical CO_2 reduction is superior to electrochemical reduction with respect to the formation of Ru−$C(O)NMe_2$ as the precursor to DMF. Reductive CO_2 activation on metals followed by oxidative activation of the resultant M−CO combines established CO_2 and CO chemistry and can lead to new a technology for organic synthesis using CO_2 as a C1 building block.

Scheme 4. Proposed Reaction Mechanism for Dialkylformamide and HCOOH Generation in Photochemical CO_2 Reduction

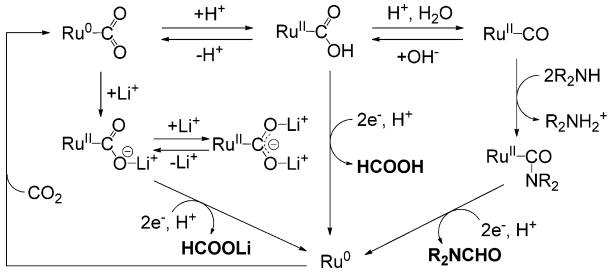

CO_2 FIXATION TO CARBONYL CARBON OF THIOESTERS

In biological CO_2 fixation, CO_2 is introduced to an organic moiety with C−C bond formation. Photosynthetic bacteria fix four CO_2 molecules in one turn of the reductive carboxylic acid cycle.[72−78] Two of the molecules are fixed to the carbonyl carbon of acetyl coenzyme A and succinyl coenzyme A to generate pyruvate and α-keto glutarate, respectively (eq 7), where reduced ferredoxins provide electrons required in the reaction.

$$RC(O)SCoA + CO_2 + 2e^- \rightarrow RC(O)COO^- + CoAS^- \quad (7)$$

$$(R = CH_3,\ HOOCCH_2CH_2;\ CoA = \text{coenzyme A})$$

In 1975, Tabushi et al. reported that $C_6H_5CH_2C(O)SC_8H_{17}$ reacted with CO_2 in the presence of $[Fe(S_2C_2Ph_2)_2]_2$, $Na_2S_2O_4$, $NaHCO_3$, and NH_3 to form $C_6H_5CH_2CH(NH_2)COO^-$ (0.3% yield) through $C_6H_5CH_2C(O)COO^-$, where $[Fe(S_2C_2Ph_2)_2]_2$ was used as the electron donor in place of ferredoxins (eq 8).[79−81]

$$C_6H_5CH_2C(O)SC_8H_{17} + CO_2 + 2e^- \rightarrow C_6H_5CH_2C(O)COO^- \xrightarrow{+NH_3} C_6H_5CH_2CH(NH_2)COO^- \quad (8)$$

However, it is still not clear whether CO_2, the substrate, or both is activated in CO_2 fixation to the positively polarized carbonyl carbon (eq 8). Synthetic 4Fe4S clusters as ferredoxin models displayed stable $[Fe_4S_4(SR)_4]^{2-/3-}$ redox couples in organic solvents. H_2O-soluble 4Fe4S clusters are subject to hydrolysis in aqueous solution. Solubilization of 4Fe4S clusters having long alkyl RS groups in aqueous micellar solutions

DOI: 10.1021/ic502745u
Inorg. Chem. 2015, 54, 5085−5095

permitted determination of the redox potentials in aqueous solution without the addition of an excess of free RS ligands to depress the hydrolysis reactions.[82] The redox potential of the $[Fe_4S_4(SR)_4]^{2-/3-}$ couple (R = $C_6H_5C_4H_9$, $C_6H_5C_8H_{17}$) in micellar solutions shifted by −60 mV/pH at pH values of less than ca. 9 because of participation of one proton in the redox reaction.[83] A comparison of the redox behavior among the series of $[Fe_4X_4(YR)_4]^{2-/3-}$ couples (XY = SS, SSe, SeS, and SeSe) in aqueous micellar solutions revealed the occurrence of reversible protonation of the core S of $[Fe_4S_4(SR)_4]^{3-}$ and the terminal RS of $[Fe_4S_4(SR)_4]^{2-}$ with pK_a values of 8.8 and 5.85, respectively (Figure 5).[84,85] CO_2 is readily trapped on strongly

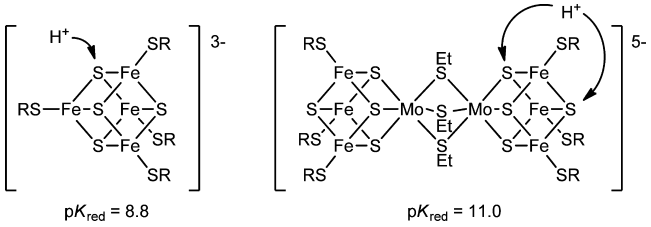

Figure 5. Protonation sites of $[Fe_4S_4(SR)_4]^{3-}$ and $[Fe_6Mo_2S_8(SR)_9]^{5-}$.

basic sites. Accordingly, basic ligands linked to redox centers can provide suitable sites for reductive activation of CO_2 aimed at incorporation to organic groups with holding of the scaffold because M−η^1-CO_2 complexes easily undergo reductive C−O bond cleavage under CO_2. The basicity of the core and terminal sulfur atoms of $[Fe_4S_4(SR)_4]^{3-}$ and $[Fe_4S_4(SR)_4]^{2-}$ was not sufficient to accept an electrophilic attack of CO_2. Indeed, the CV plots of $[Fe_4S_4(SR)_4]^{2-}$ in CH_3CN under CO_2 and N_2 were consistent with each other. A double cubane $[Fe_6Mo_2S_8(SR)_9]^{3-}$ with two $MoFe_3S_4$ cores and three μ_2-SR bridges displayed a stable (3−/4−/5−) redox couple in CH_3CN and DMF.[86] Plots of the redox potentials of FeMoS clusters having long alkyl chains versus the pH in an aqueous micellar solution shifted by −30 mV/pH at a pH lower than 11, indicating the participation of one proton in the $[Fe_6Mo_2S_8(SR)_9]^{3-/5-}$ redox reactions.[87] Despite the difference in the bridging ligand between μ_2-SEt and μ_2-OMe, similar pK_a values of $[Mo_2Fe_6(\mu_3\text{-}X)_3(SC_6H_4C_8H_{17})_6]^{5-}$ were ascribed to reversible protonation on one of the core sulfur atoms of the Fe_3MoS_4 scaffolds.[87] The basicity of the core sulfur of $[Fe_6Mo_2S_8(SR)_9]^{5-}$ (pK_a 11; Figure 5) was strong enough to form a CO_2 adduct in dry CH_3CN. Because the cathodic peak current of the $[Fe_6Mo_2S_8(SR)_9]^{4-/5-}$ redox couple ($E_{1/2}$ = −1.46 V) increased after CO_2 bubbling in the solution at 5 mV/s in CH_3CN (Figure 6),[88] an increase in the cathodic current of the (4−/5−) redox couple was not observed at a sweep rate of 100 mV/s possibly because of slow adduct formation. The removal of CO_2 from the solution by N_2 bubbling completely regenerated the original CV under N_2. Taking into account the coordinatively saturated hexacoordinated molybdenum and the formal oxidation states of Fe^{II} or Fe^{III} in $[Fe_6Mo_2S_8(SR)_9]^{5-}$, the possibility of CO_2 attack on those metal ions can be ruled out. The addition of an excess of MeC(O)SEt to the CH_3CN solution of $[Fe_6Mo_2S_8(SEt)_9]^{3-}$ under CO_2 caused strong catalytic currents at potentials more negative than −1.4 V. Alternatively, the addition of MeC(O)SEt to $[Fe_6Mo_2S_8(SEt)_9]^{3-}$ under N_2 did not influence the CV. The strong catalytic currents that flowed only when CO_2 and MeC(O)SEt coexisted indicates that $[Fe_6Mo_2S_8(SEt)_9]^{5-}$ catalyzed the reaction of CO_2 with MeC(O)SEt. The

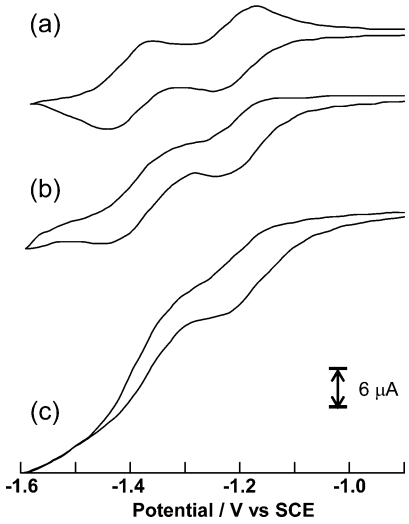

Figure 6. CV plots of $[Fe_6Mo_2S_8(SEt)_9]^{3-}$ in CH_3CN under (a) N_2 and (b) CO_2 and (c) in the presence of MeC(O)SEt under CO_2 (dE/dt = 5 mV).

controlled potential electrolysis of $[Fe_6Mo_2S_8(SEt)_9]^{3-}$ in the presence of EtC(O)SEt and a 3 Å molecular sieve as a dehydration agent in CH_3CN at −1.65 V (vs SCE) catalytically produced $EtC(O)COO^-$ (eq 9).

$$RC(O)SEt + CO_2 + 2e^- \rightarrow RC(O)COO^- + EtS^- \quad (9)$$

(R = CH_3, C_2H_5, C_6H_5)

Electrolysis, however, completely stopped after generation of about 600% $EtC(O)COO^-$ because the accumulation of EtS^- generated as a byproduct in the reaction strongly disrupted α-keto acid formation (eq 9). Note that $[Mo_2Fe_6S_8(SPh)_9]^{5-}$ also interacted with CO_2 in the CV plot similar to $[Mo_2Fe_6S_8(SEt)_9]^{5-}$. However, $[Fe_6Mo_2S_8(SPh)_9]^{5-}$ could not catalyze CO_2 fixation (eq 9). Such a distinct difference between $[Mo_2Fe_6S_8(SEt)_9]^{5-}$ and $[Mo_2Fe_6S_8(SPh)_9]^{5-}$ toward CO_2 fixation was due to the lability of terminal EtS of the former to substitution with other thiolate molecules and the complete inertness of PhS of the latter to substitution reactions. The catalytic formation of $RC(O)COO^-$ through CO_2 fixation on the carbonyl carbon of RC(O)SEt (R = CH_3, C_2H_5, and C_6H_5) was ascribed to the coupling of CO_2 bonded on μ_3-S and RC(O)SEt ligated on iron of $[Mo_2Fe_6S_8(SEt)_9]^{5-}$ with regeneration of $[Mo_2Fe_6S_8(SEt)_9]^{3-}$ and free EtS^- (Scheme 5).

■ OXALATE FORMATION

Reactions of CO_2 with two-electron-reduced forms of trinuclear $[(Cp'M)_3(\mu_3\text{-}S)_2]^{2+}$ [Cp′ = CpMe (methylcyclopentadienyl), $CpMe_5$ (pentamethylcyclopentadienyl); M = Co, Rh, Ir] were conducted along with elucidation of the reactivity of CO_2 activated on μ_3-S of $[Mo_2Fe_6(SEt)_9]^{5-}$ (eq 9).[89,90] The crystal structures of $[(CpMeCo)_3(\mu_3\text{-}S)_2]^{n+}$ ($[Co_3S_2]^{n+}$; n = 2, 1, 0; Cp = cyclopentadienyl) revealed that one of the three Co−Co bond lengths was elongated from 2.52 to 2.87 Å upon one-electron reduction of $[Co_3S_2]^{2+}$ and cleaved in $[Co_2S_2]^0$ (Figure 7).[89] The structural changes occurring as reduction of the Co_3S_2 framework progressed resulted from the accumulation of electrons into the Co−Co σ^* bond of the lowest unoccupied molecular orbital of $[Co_3S_2]^{2+}$. Analogous $[(CpMe_5Rh)_3(\mu_3\text{-}S)_2]^{2+}$ ($[Rh_3S_2]^{2+}$) and $[(CpMe_5Ir)_3(\mu_3\text{-}S)_2]^{2+}$ ($[Ir_3S_2]^{2+}$) complexes also displayed two reversible

DOI: 10.1021/ic502745u
Inorg. Chem. 2015, 54, 5085−5095

Scheme 5. Proposed Mechanism for α-Keto Acid Formation through Fixation of CO_2 to Carbonyl Carbon of Thioesters

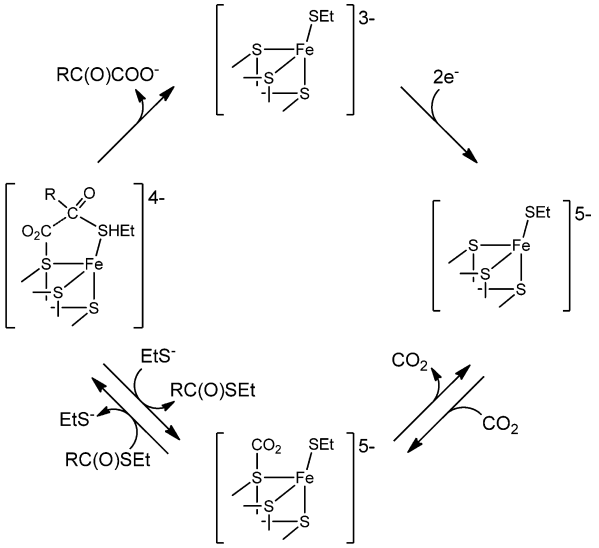

$[M_3S_2]^{2+/1+/0}$ redox couples at $E_{1/2}$ = −0.52 and −0.91 V (Rh)[91] and −0.83 and −0.98 V (Ir)[92,93] in CH_3CN under N_2. Controlled potential electrolysis of $[Co_3S_2]^{2+}$ at −0.70 V in CH_3CN containing Me_4NBr under CO_2 precipitated white $(Me_4N)_2C_2O_4$ with a current efficiency of 80%, although electrolysis stopped completely after 60 C passed because of deposition of $(Me_4N)_2C_2O_4$ on the surface of a gas carbon working electrode (eq 10).[94]

$$CO_2 + 2e^- \rightarrow C_2O_4^{2-} \quad (10)$$

Similarly, electrolysis of $[Rh_3S_2]^{2+}$ at −1.50 V in CO_2-saturated CH_3CN under the same conditions also catalytically produced $(Me_4N)_2C_2O_4$ with a current efficiency of 60%.[91] The rate of CO_2 reduction by $[Co_3S_2]^0$ and $[Rh_3S_2]^0$ was too slow to detect the current changes on the CV time scale. In contrast, $[Ir_3S_2]^0$ prepared by electrolysis of $[Ir_3S_2](BPh_4)_2$ at −1.30 V in the presence of Me_4NBr rapidly reacted with CO_2, and orange $[(IrCpMe_5)_2(IrCpMe_5CH_2CN)S_2](BPh_4)$ ($[Ir_3CH_2CN]^+$) was isolated together with $(Me_4N)_2C_2O_4$ precipitate (70% yield) from the electrolyte solution (eq 11).[95] Electrolysis of $[Ir_3S_2](BPh_4)_2$ in the presence of Me_4NBF_4 in CH_3CN at −1.30 V under CO_2 also produced $(Me_4N)_2C_2O_4$ and $[(Ir_3CH_2CN)]^+$. The crystal structure of $[(Ir_3CH_2CN)(\mu_3\text{-}S)_2]^+$ clarified that two iridium atoms of the Ir_3S_2 framework are surrounded by η^5-$CpMe_5$ and the remaining iridium is coordinated with η^4-$CpMe_5CH_2CN$, possibly formed by an attack of CH_2CN^- to the $CpMe_5$ ring (Figure 8).

$$[(IrCpMe_5)_3(\mu_3\text{-}S)_2]^0 + CH_3CN + 2CO_2 \rightarrow [(IrCp^*)_2(Ir - \eta^4\text{-}CpMe_5CH_2CN)(\mu_3\text{-}S)_2]^+ + C_2O_4^{2-} + H^+ \quad (11)$$

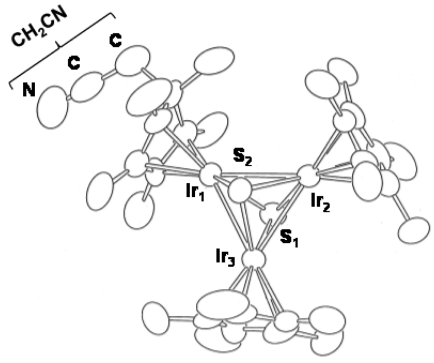

Figure 8. X-ray crystal structure of $[(IrCpMe_5)_2(Ir\text{-}\eta^4\text{-}CpMe_5CH_2CN)(\mu_3\text{-}S)_2]^+$ ($[Ir_3CH_2CN]^+$; hydrogen atoms omitted for clarity).

The CV of $[Ir_3S_2CH_2CN](BPh_4)$ showed one reversible $[Ir_3S_2CH_2CN]^{+/0}$ redox couple ($E_{1/2}$ = −1.45 V; eq 12) followed by one irreversible cathodic wave (E_{cp} = −1.83 V) in the cathodic potential sweep under N_2. In the reverse anodic potential sweep, the $[Ir_3S_2]^{0/1+/2+}$ redox couples emerged at E_{ap} = −0.93 and −0.78 V in addition to the $[Ir_3S_2CH_2CN]^{+/0}$ couple at $E_{1/2}$ = −1.45 V (Figure 9a), indicating that two-

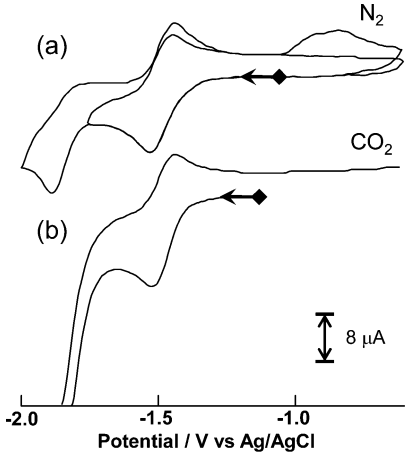

Figure 9. CV plots of $[(IrCpMe_5)_2(Ir\text{-}\eta^4\text{-}CpMe_5CH_2CN)(\mu_3\text{-}S)_2]^+$ under (a) N_2 and (b) CO_2 (dE/dt = 100 mV).

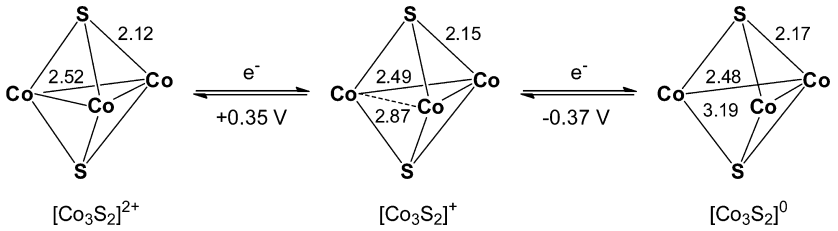

Figure 7. Structural changes in $[(CpMeCo)_3(\mu_3\text{-}S)_2]^{n+}$ ($[Co_3S_2]^{n+}$; n = 2, 1, 0) occurring during redox reaction.

DOI: 10.1021/ic502745u
Inorg. Chem. 2015, 54, 5085−5095

electron reduction of $[Ir_3S_2CH_2CN]^+$ resulted in dissociation of CH_2CN^- with regeneration of $[Ir_3S_2]^{2+}$ under N_2 (eq 13).

$$[Ir_3S_2CH_2CN]^+ + e^- \rightleftarrows [Ir_3S_2CH_2CN]^0 \quad (12)$$

$$[Ir_3S_2CH_2CN]^0 + e^- \rightarrow [Ir_3S_2CH_2CN]^0 + [CH_2CN]^- \quad (13)$$

However, bubbling CO_2 into the CH_3CN solution caused strong catalytic currents at potentials more negative than −1.65 V because of $C_2O_4^{2-}$ generation (Figure 9b). At the same time, the $[Ir_3S_2]^{2+/1+/0}$ redox couples did not appear in the CV plot. Thus, the two electrons transferred to $[Ir_3S_2CH_2CN]^+$ were effectively consumed in the formation of $C_2O_4^{2-}$ under CO_2. Treatment of $[Ir_3S_2CH_2CN]^+$ with aqueous HCl also produced $[Ir_3S_2]^{2+}$ in quantitative yield while liberating CH_2CN in CH_2Cl_2 under N_2.

The IR spectra of $[Ir_3S_2CH_2CN](BPh_4)$ in CD_3CN under $^{12}CO_2$ and $^{13}CO_2$ exhibited a strong band at 1682 and 1632 cm^{-1}, respectively. Evaporation of the solvent restored the original IR spectra of $[Ir_3S_2CH_2CN]^+$ (eq 14). Furthermore, electrolysis of $[Ir_3S_2CH_2CN](BPh_4)$ at −1.50 V in CD_3CN under $^{12}CO_2$ and $^{13}CO_2$ resulted in the appearance of new bands at 1603 and 1561 cm^{-1}, respectively, and the original 1682 cm^{-1} ($^{12}CO_2$) and 1632 cm^{-1} ($^{13}CO_2$) bands shifted slightly to lower wavenumbers (Figure 10). Prolonged

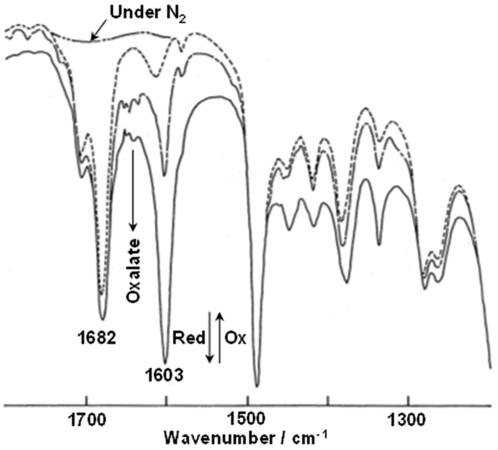

Figure 10. IR electrospectrochemistry of $[(IrCMe_5)_2(IrCpMe_5CH_2CN)(\mu_3\text{-}S)_2]^+$ in the presence and absence of $^{12}CO_2$.

electrolysis caused the appearance of strong $\nu(CO_2)$ bands of $^{12}C_2O_4^{2-}$ (1633 and 1397 cm^{-1}) and $^{13}C_2O_4^{2-}$ (1601 and 1366 cm^{-1}), respectively (eq 15; Figure 10).

$$[Ir_3S_2CH_2CN]^+ + CO_2 \rightleftarrows \{[Ir_3S_2CH_2CN](CO_2)\}^+ \quad (14)$$

$$\{[Ir_3S_2CH_2CN](CO_2)\}^+ + CO_2 + e^- \rightleftarrows [Ir_3S_2CH_2CN](CO_2)_2 \quad (15)$$

These results were explained by the 1:1 and 1:2 adducts of $[Ir_3S_2CH_2CN]^+$ and $[Ir_3S_2CH_2CN]^0$, respectively, with CO_2 before production of $C_2O_4^{2-}$. The OCO angles of the 1:1 and 1:2 adducts were estimated using eq 16, with the assumption of CO_2 complex coordination in η^1-CO_2 mode.

$$\left(\frac{\nu^i}{\nu}\right)^2 = \left(\frac{M_c}{M_c^i}\right)\left(\frac{M_c^i + 2M_o \sin^2\alpha}{M_c + 2M_o \sin^2\alpha}\right) \quad (16)$$

Here, ν^i and ν represent the $\nu(^{13}CO_2)$ and $\nu(^{12}CO_2)$ bands (cm^{-1}) and M_c^i, M_c, and M_o are the mass numbers of ^{13}C, ^{12}C, and ^{16}O, respectively.[96]

The OCO angles of the first and second CO_2 molecules linked to $[Ir_3S_2CH_2CN]^+$ and $[Ir_3S_2CH_2CN]^0$ were calculated as 157° and 132°, respectively. The latter is close to the OCO angle of $[Co(Pr\text{-}salen)(\eta^1\text{-}CO_2Na)]^+$ (135°),[97] although those of $RhCl(diars)(\eta^1\text{-}CO_2)$[98] and $[Ru(bpy)_2(CO)(\eta^1\text{-}CO_2)]$ were 126° and 120°, respectively. The binding site of CO_2 was assumed at μ_3-S of $[Ir_3S_2CH_2CN]^+$ because three iridium atoms were coordinatively saturated. One-electron reduction of $\{[Ir_3S_2CH_2CN](CO_2)\}^+$ would cleave one Ir−Ir bond, similar to the behavior of $[(CoCpMe)_3(\mu_3\text{-}S)_2]^0$. The resulting coordinatively unsaturated iridium probably formed binding sites for the electrophilic attack of the second CO_2. Further one-electron reduction of the 1:2 adduct presumably facilitated coupling of the two CO_2 molecules activated on the cluster to produce $C_2O_4^{2-}$ with regeneration of $[Ir_3S_2CH_2CN]^+$ (eq 17). Note that reductive activation of CO_2 on two-electron-reduced metal complexes usually results in CO evolution through metal−CO bond cleavage. In contrast, the electron density of the two CO_2 molecules activated on the two-electron-reduced M_3S_2 scaffold is apparently not enough to produce oxide transfer to CO_2. The inability to produce CO during CO_2 reduction catalyzed by the M_3S_2 clusters allowed the activation of two CO_2 molecules on the M_3S_2 core.

$$[Ir_3S_2CH_2CN]^0(CO_2)_2 + e^- \rightarrow [Ir_3S_2CH_2CN]^+ + C_2O_4^{2-} \quad (17)$$

CONCLUSIONS

Reductive conversion from CO_2 to CO on metal complexes is caused by acid−base equilibrium or disproportionation of metal−η^1-CO_2 under CO_2. Successive protonation of M−η^1-CO_2 under protic conditions results in M−COOH and M−CO formation, which serve as precursors to HCOOH and CO generation in photo- and electrochemical CO_2 reduction. Attacks of nucleophiles to M−CO have fundamental importance for the incorporation of CO into organic molecules, so that reductive cleavage of the M−CO bonds derived from CO_2 is the largest barrier for utilization of CO_2 as a C1 building block in organic synthesis. Visible-light irradiation to a catalytic system composed of $[Ru(bpy)_2(CO)_2]^{2+}$/$[Ru(bpy)_3]^{2+}$/Me_2NH/$Me_2NH_2^+$ as a catalyst, a photosensitizer, a proton donor, and a nuceophile in addition to an electron source, respectively, in CO_2-saturated CH_3CN catalytically produced DMF in photochemical CO_2 reduction. Smooth conversion from $[Ru(bpy)_2(CO)(CO_2)]^0$ to $[Ru(bpy)_2(CO)_2]^{2+}$ in the presence of $Me_2NH_2^+$ followed by rapid formation of $[Ru(bpy)_2(CO)(CONMe_2)]^+$ through the attack of Me_2NH to $[Ru(bpy)_2(CO)_2]^{2+}$ permitted selective DMF generation in the reduction of CO_2 for the first time. Structurally robust μ_3-S of reduced metal−sulfur clusters provided a suitable site for reductive activation of CO_2 with retention of the framework. Successful catalytic α-keto acid production via CO_2 fixation to the positively polarized carbonyl carbon of thioesters was ascribed to the reaction of CO_2 activated on μ_3-S of $[Fe_6Mo_2S_8(SEt)_3]^{5-}$ with thioesters trapped on an adjacent

DOI: 10.1021/ic502745u
Inorg. Chem. 2015, 54, 5085−5095

iron of the cluster. Furthermore, two-electron reduction of $[(CpMe_n)_3M_3S_2]^{2+}$ (n = 1, M = Co; n = 5, M = Rh, Ir) resulted in cleavage of one of the M−M bonds, which created a reaction site (space) for the coupling reaction of two CO_2 possibly activated on μ_3-S and a metal ion to produce oxalate catalytically.

We have presented reduction of CO_2 accompanied by C−N and C−C bond formation aimed at utilization of CO_2 as a C1 building block. The common character in those CO_2 reductions is reductive activation of CO_2 with the η^1 binding mode on metals and/or bridging sulfur ligands, which would provide a fundamental concept for utilization of CO_2 as a C1 building block in organic synthesis.

AUTHOR INFORMATION

Corresponding Author

*E-mail: koji.tanaka@icems.kyoto-u.ac.jp.

Notes

The authors declare no competing financial interest.

REFERENCES

(1) Fournier, J.; Bruneau, C.; Dixneuf, P. H.; Lécolier, S. *J. Org. Chem.* **1991**, *56*, 4456.
(2) Mahé, R.; Sasaki, Y.; Bruneau, C.; Dixneuf, P. H. *J. Org. Chem.* **1989**, *54*, 1518.
(3) Nomura, R.; Hasegawa, Y.; Ishimoto, M.; Toyosaki, T.; Matsuda, H. *J. Org. Chem.* **1992**, *57*, 7339.
(4) Kihara, N.; Endo, T. *Macromolecules* **1992**, *25*, 4824.
(5) Halmann, M. H.; Steinberg, M. *Greenhouse gas carbon dioxide mitigation*; Lewis Publishers: Boca Raton, FL, 1991.
(6) Tokuda, M. *J. Nat. Gas Chem.* **2006**, *15*, 275.
(7) Matthessen, R.; Fransaer, J.; Binnemans, K.; Vos, D. E. D. *Beilstein J. Org. Chem.* **2014**, *10*, 2484.
(8) Zhao, S.-F.; Horne, M.; Bond, A. M.; Zhang, J. *Green Chem.* **2014**, *16*, 2242.
(9) Tateno, H.; Nakabayashi, K.; Kashiwagi, T.; Senboku, H.; Atobe, M. *Electrochim. Acta* **2015**, *161*, 212.
(10) Amatore, C.; Jutand, A.; Nielsen, M. F. *J. Am. Chem. Soc.* **1992**, *114*, 7076.
(11) Amatore, C.; Jutand, A. *J. Am. Chem. Soc.* **1991**, *113*, 2819.
(12) Sayyed, F. B.; Sakaki, S. *Chem. Commun.* **2014**, *50*, 13026.
(13) Liu, Y.; Cornella, J.; Martin, R. *J. Am. Chem. Soc.* **2014**, *136*, 11212.
(14) Guan, W.; Sayyed, F. B.; Zeng, G.; Sakaki, S. *Inorg. Chem.* **2014**, *53*, 6444.
(15) Ishida, H.; Tanaka, K.; Tanaka, T. *Organometallics* **1987**, *6*, 181.
(16) Tanaka, K. *Bull. Chem. Soc. Jpn.* **1998**, *71*, 17.
(17) Ishida, H.; Fujiki, K.; Ohba, T.; Ohkubo, K.; Tanaka, K.; Terada, T.; Tanaka, T. *J. Chem. Soc., Dalton Trans.* **1990**, 2155.
(18) Tanaka, K.; Ooyama, D. *Coord. Chem. Rev.* **2002**, *226*, 211.
(19) Tanaka, K.; Morimoto, M.; Tanaka, T. *Chem. Lett.* **1983**, 901.
(20) Ishida, H.; Tanaka, K.; Morimoto, M.; Tanaka, T. *Organometallics* **1986**, *5*, 724.
(21) Tanaka, K. *Chem. Rec.* **2009**, *9*, 169.
(22) Kobayashi, K.; Tanaka, K. *Phys. Chem. Chem. Phys.* **2014**, *16*, 2240.
(23) Tanaka, H.; Nagao, H.; Peng, S.-M.; Tanaka, K. *Organometallics* **1992**, *11*, 1450.
(24) Tanaka, H.; Tzeng, B.-C.; Nagao, H.; Peng, S.-M.; Tanaka, K. *Inorg. Chem.* **1993**, *32*, 1508.
(25) Toyohara, K.; Nagao, H.; Adachi, T.; Yoshida, T.; Tanaka, K. *Chem. Lett.* **1996**, 27.
(26) Ishida, H.; Tanaka, H.; Tanaka, K.; Tanaka, T. *J. Chem. Soc., Chem. Commun.* **1987**, 131.
(27) Collomb-Dunand-Sauthier, M.-N.; Deronzier, A.; Ziessel, R. *Inorg. Chem.* **1994**, *33*, 2961.
(28) Chardon-Noblat, S.; Deronzier, A.; Ziessel, R.; Zsoldos, D. *Inorg. Chem.* **1997**, *36*, 5384.
(29) Chardon-Noblat, S.; Collmb-Dunand-Sauthier, M.-N.; Deronzier, A.; Ziessel, R.; Zsoldos, D. *Inorg. Chem.* **1994**, *33*, 4410.
(30) Chardon-Noblat, S.; Deronzier, A.; Ziessel, R.; Zsoldos, D. *J. Electroanal. Chem.* **1998**, *444*, 253.
(31) Tamaki, Y.; Morimoto, T.; Koike, K.; Ishitani, O. *Proc. Natl. Acad. Sci. U.S.A.* **2012**, *109*, 15673.
(32) Ishida, H.; Terada, T.; Tanaka, K.; Tanaka, T. *Inorg. Chem.* **1990**, *29*, 905.
(33) Ishida, H.; Tanaka, K.; Tanaka, T. *Chem. Lett.* **1988**, 339.
(34) Nakajima, H.; Tsuge, K.; Toyohara, K.; Tanaka, K. *J. Organomet. Chem.* **1998**, *569*, 61.
(35) Nakajima, H.; Tsuge, K.; Tanaka, K. *Chem. Lett.* **1997**, 485.
(36) Reinking, M. K.; Ni, J.; Fanwick, P. E.; Kubiak, C. P. *J. Am. Chem. Soc.* **1989**, *111*, 6459.
(37) Nakajima, H.; Kushi, Y.; Nagao, H.; Tanaka, K. *Organometallics* **1995**, *14*, 5093.
(38) Lee, G. R.; Cooper, N. J. *Organometallics* **1985**, *4*, 794.
(39) Lee, G. R.; Maher, J. M.; Cooper, N. J. *J. Am. Chem. Soc.* **1987**, *109*, 2956.
(40) Ratliff, K. S.; Lentz, R. E.; Kubiak, C. P. *Organometallics* **1992**, *11*, 1986.
(41) Allen, O. R.; Dalgarno, S. J.; Field, L. D. *Organometallics* **2008**, *27*, 3328.
(42) Hawecker, J.; Lehn, J.-M.; Ziessel, R. *J. Chem. Soc., Chem. Commun.* **1984**, 328.
(43) Sullivan, B. P.; Bolinger, C. M.; Conrad, D.; Vining, W. J.; Meyer, T. J. *J. Chem. Soc., Chem. Commun.* **1985**, 1414.
(44) Kutal, C.; Weber, M. A.; Ferraudi, G.; Geiger, D. *Organometallics* **1985**, *4*, 2161.
(45) Smieja, J. M.; Kubiak, C. P. *Inorg. Chem.* **2010**, *49*, 9283.
(46) Sato, S.; Ishitani, O. *Coord. Chem. Rev.* **2015**, *282*−*283*, 50.
(47) Morris, A. J.; Meyer, G. J.; Fujita, E. *Acc. Chem. Res.* **2009**, *42*, 1983.
(48) Keith, J. A.; Grice, K. A.; Kubiak, C. P.; Carter, E. A. *J. Am. Chem. Soc.* **2013**, *135*, 15823.
(49) Smieja, J. M.; Benson, E. E.; Kumar, B.; Grice, K. A.; Seu, C. S.; Miller, A. J. M.; Mayer, J. M.; Kubiak, C. P. *Proc. Natl. Acad. Sci. U.S.A.* **2012**, *109*, 15646.
(50) Sampson, M. D.; Froehlich, J. D.; Smieja, J. M.; Benson, E. E.; Sharp, I. D.; Kubiak, C. P. *Energy Environ. Sci.* **2013**, *6*, 3748.
(51) Machan, C. W.; Chabolla, S. A.; Yin, J.; Gibson, M. K.; Tezcan, F. A.; Kubiak, C. P. *J. Am. Chem. Soc.* **2014**, *136*, 14598.
(52) Kou, Y.; Nabetani, Y.; Masui, D.; Shimada, T.; Takagi, S.; Tachibana, H.; Inoue, H. *J. Am. Chem. Soc.* **2014**, *136*, 6021.
(53) Doherty, M. D.; Grills, D. C.; Muckerman, J. T.; Polyansky, D. E.; Fujita, E. *Coord. Chem. Rev.* **2010**, *254*, 2472.
(54) Hayashi, Y.; Kita, S.; Brunschwig, B. S.; Fujita, E. *J. Am. Chem. Soc.* **2003**, *125*, 11976.
(55) Sato, S.; Koike, K.; Inoue, H.; Ishitani, O. *Photochem. Photobiol. Sci.* **2007**, *6*, 454.
(56) Takeda, H.; Koike, K.; Inoue, H.; Ishitani, O. *J. Am. Chem. Soc.* **2008**, *130*, 2023.
(57) Bian, Z.-Y.; Sumi, K.; Furue, M.; Sato, S.; Koike, K.; Ishitani, O. *Inorg. Chem.* **2008**, *47*, 10801.
(58) Takeda, H.; Ohashi, M.; Tani, T.; Ishitani, O.; Inagaki, S. *Inorg. Chem.* **2010**, *49*, 4554.
(59) Yamamoto, Y.; Tamaki, Y.; Yui, T.; Koike, K.; Ishitani, O. *J. Am. Chem. Soc.* **2010**, *132*, 11743.
(60) Takeda, H.; Ishitani, O. *Coord. Chem. Rev.* **2010**, *254*, 346.
(61) Morimoto, T.; Nishiura, C.; Tanaka, M.; Rohacova, J.; Nakagawa, Y.; Funada, Y.; Koike, K.; Yamamoto, Y.; Shishido, S.; Kojima, T.; Saeki, T.; Ozeki, T.; Ishitani, O. *J. Am. Chem. Soc.* **2013**, *135*, 13266.
(62) Tamaki, Y.; Koike, K.; Morimoto, T.; Ishitani, O. *J. Catal.* **2013**, *304*, 22.
(63) Morimoto, T.; Nakajima, T.; Sawa, S.; Nakanishi, R.; Imori, D.; Ishitani, O. *J. Am. Chem. Soc.* **2013**, *135*, 16825.

DOI: 10.1021/ic502745u
Inorg. Chem. 2015, 54, 5085−5095

(64) Nagao, H.; Mizukawa, T.; Tanaka, K. *Chem. Lett.* **1993**, 955.
(65) Nagao, H.; Mizukawa, T.; Tanaka, K. *Inorg. Chem.* **1994**, *33*, 3415.
(66) Toyohara, K.; Nagao, H.; Mizukawa, T.; Tanaka, K. *Inorg. Chem.* **1995**, *34*, 5399.
(67) Toyohara, K.; Tsuge, K.; Tanaka, K. *Organometallics* **1995**, *14*, 5099.
(68) Ooyama, D.; Tomon, T.; Tsuge, K.; Tanaka, K. *J. Organomet. Chem.* **2001**, *619*, 299.
(69) Jetz, W.; Angelici, R. J. *J. Am. Chem. Soc.* **1972**, *94*, 3799.
(70) Ishida, H.; Tanaka, H.; Tanaka, K.; Tanaka, T. *Chem. Lett.* **1987**, 597.
(71) Kobayashi, K.; Kikuchi, T.; Kitagawa, S.; Tanaka, K. *Angew. Chem., Int. Ed.* **2014**, *53*, 11813.
(72) Evans, M. C. W.; Buchanan, B. B.; Arnon, D. I. *Proc. Natl. Acad. Sci. U.S.A.* **1966**, *55*, 928.
(73) Kusai, A.; Yamanaka, T. *Biochem. Biophys. Acta* **1973**, *292*, 621.
(74) Bachofen, R.; Buchanan, B. B.; Arnon, D. I. *Proc. Natl. Acad. Sci. U.S.A.* **1964**, 690.
(75) Buchanan, B. B.; Bachofen, R.; Arnon, D. I. *Proc. Natl. Acad. Sci. U.S.A.* **1964**, *52*, 839.
(76) Evans, M. C. W. *Biochem. Biophys. Res. Commun.* **1968**, *33*, 146.
(77) Gottschalk, G.; Chowdhury, A. A. *FEBS Lett.* **1969**, *2*, 342.
(78) Thauer, R. K.; Rupprecht, E.; Jungcrmann, K. *FEBS Lett.* **1970**, *8*, 304.
(79) Nakajima, T.; Yabushita, Y.; Tabushi, I. *Nature* **1975**, *256*, 60.
(80) Tabushi, I.; Yabushita, Y.; Nakajima, T. *Tetrahedron Lett.* **1976**, *17*, 4343.
(81) Kubota, Y.; Kodaka, M.; Tomohiro, T.; Okuno, H. *Chem. Express* **1991**, 487.
(82) Tanaka, K.; Tanaka, T.; Kawafune, I. *Inorg. Chem.* **1984**, *25*, 516.
(83) Tanaka, K.; Masanaga, M.; Tanaka, T. *J. Am. Chem. Soc.* **1986**, *108*, 5448.
(84) Nakamoto, M.; Tanaka, K.; Tanaka, T. *J. Chem. Soc., Chem. Commun.* **1986**, 1669.
(85) Nakamoto, M.; Tanaka, K.; Tanaka, T. *Bull. Chem. Soc. Jpn.* **1988**, *61*, 4099.
(86) Christou, G.; Garner, C. D. *J. Chem. Soc., Dalton Trans.* **1980**, 2354.
(87) Tanaka, K.; Moriya, M.; Tanaka, T. *Inorg. Chem.* **1986**, *25*, 835.
(88) Komeda, N.; Nagao, H.; Matsui, T.; Adachi, G.; Tanaka, K. *J. Am. Chem. Soc.* **1992**, 3625.
(89) Pulliam, C. R.; Thoden, J. B.; Stacy, A. M.; Spencer, B.; Englert, M. H.; Dahl, L. F. *J. Am. Chem. Soc.* **1991**, *113*, 7398.
(90) Sorai, M.; Kosaki, A.; Suga, H.; Seki, S.; Yoshida, T.; Otsuka, S. *Bull. Chem. Soc. Jpn.* **1971**, *44*, 2364.
(91) Kushi, Y.; Nagao, H.; Nishioka, T.; Isobe, K.; Tanaka, K. *Chem. Lett.* **1994**, 2175.
(92) Nishioka, T.; Isobe, K. *Chem. Lett.* **1994**, 1661.
(93) Venturelli, A.; Rauchfuss, T. B. *J. Am. Chem. Soc.* **1994**, *116*, 4824.
(94) Kushi, Y.; Nagao, H.; Nishioka, T.; Isobe, K.; Tanaka, K. *J. Chem. Soc., Chem. Commun.* **1995**, 1223.
(95) Tanaka, K.; Kushi, Y.; Tsuge, K.; Toyohara, K.; Nishioka, T.; Isobe, K. *Inorg. Chem.* **1998**, *37*, 120.
(96) Nakamoto, K. *Infrared and Raman Spectra of Inorganic and Coordination Compounds*; Wiley-Interscience Publications: New York, 1986.
(97) Gambarotta, S.; Arena, F.; Floriani, C.; Zanazzi, P. F. *J. Am. Chem. Soc.* **1982**, *104*, 5082.
(98) Calabrese, J. C.; Herskovitz, T.; Kinney, J. B. *J. Am. Chem. Soc.* **1983**, *105*, 5914.

DOI: 10.1021/ic502745u
Inorg. Chem. 2015, 54, 5085−5095